The central role of ocean dynamics in connecting the North Atlantic Oscillation to the Atlantic Multidecadal Oscillation

Thomas L. Delworth[1], Fanrong Zeng[1], Liping Zhang[1], Rong Zhang[1], Gabriel A. Vecchi[1], and Xiaosong Yang[1]

[1]Geophysical Fluid Dynamics Laboratory/NOAA

201 Forrestal Rd.

Princeton, NJ 08540 USA

Revised version submitted to Journal of Climate

September 23, 2016

Corresponding author: Thomas L. Delworth

E-Mail: tom.delworth@noaa.gov
Phone: 609-452-6565

Postal:
Geophysical Fluid Dynamics Laboratory/NOAA
201 Forrestal Rd.
Princeton University Forrestal Campus
Plainsboro, NJ 08540
USA

Abstract

The relationship between the North Atlantic Oscillation (NAO) and Atlantic sea surface temperature (SST) variability is investigated using models and observations. Coupled climate models are used in which the ocean component is either a fully dynamic ocean, or a slab ocean with no resolved ocean heat transport. On time scales less than ten years NAO variations drive a tripole pattern of SST anomalies in both observations and models. This SST pattern is a direct response of the ocean mixed layer to turbulent surface heat flux anomalies associated with the NAO.

On time scales longer than ten years a similar relationship exists between the NAO and the tripole pattern of SST anomalies in models that use a slab ocean. A different relationship exists both for the observations and for models with a dynamic ocean. In these models a positive (negative) NAO anomaly leads, after a decadal-scale lag, to a monopole pattern of warming (cooling) that resembles the Atlantic Multidecadal Oscillation (AMO), although with smaller than observed amplitudes of tropical SST anomalies. Ocean dynamics are critical to this decadal scale response in the models. The simulated Atlantic Meridional Overturning Circulation (AMOC) strengthens (weakens) in response to a prolonged positive (negative) phase of the NAO, thereby enhancing (decreasing) poleward heat transport, leading to broad scale warming (cooling).

We use additional simulations heat flux anomalies derived from observed NAO variations from 1901 to 2014 are applied to the ocean component of coupled models. We show that ocean dynamics allow models to reproduce important aspects of the observed AMO, especially in the subpolar gyre.

1. Introduction

Numerous studies have examined sea surface temperature (SST) variability in the Atlantic and associated climatic impacts. These studies have shown that on short (interannual) time scales there exists a tripole pattern of SST anomalies that arises as a response of the oceanic mixed layer to turbulent surface heat flux anomalies driven by variations of the North Atlantic Oscillation (NAO)(Bjerknes 1964; Daly 1978; Cayan 1992; Battisti et al. 1995; Gulev et al. 2013). A more intriguing question, with greater relevance for larger-scale climate, is what drives SST variations in the Atlantic on decadal to multidecadal time scales. Analyses of both instrumental data and proxy climate reconstructions have shown the existence of a basin wide monopole SST anomaly pattern that varies on multidecadal time scales. This has been called (Kerr 2000) the Atlantic Multidecadal Oscillation (AMO), or Atlantic Multidecadal Variability (AMV), and has been linked to numerous important climate phenomena around the world. These include droughts in Africa, changing tropical storm activity in the Atlantic, and drought over interior North America. (Folland et al. 1986; Enfield et al. 2001; Sutton and Hodson 2005; Knight et al. 2006; Zhang and Delworth 2006; Chylek et al. 2009, 2014; Mahajan et al. 2011; Nigam et al. 2011; Sutton and Dong 2012; Hu and Veres 2016)

Many previous studies have hypothesized that this AMO pattern is a result of variations in ocean circulation (Bjerknes 1964) involving the Atlantic Meridional Overturning Circulation (AMOC). Extensive prior work has shown that AMOC variations occur in models on decadal to multidecadal time scales, and that these AMOC variations produce monopole SST patterns in the Atlantic that resemble the observed AMO (Delworth et al. 1993; Knight et al. 2005; Danabasoglu et al. 2012). However, models vary widely in the time scale of their AMOC and SST variability, and in the underlying mechanisms producing that AMOC variability(Grossmann and Klotzbach 2009; Keenlyside et al. 2013). Further, while the models typically produce SST patterns that resemble observations in

the subpolar gyre, the simulated anomalies are typically smaller than observed in the tropical North Atlantic. Recent work (Clement et al. 2015) has provided a different perspective, suggesting that ocean circulation changes do not play a substantial role in the observed AMO in models with a dynamic ocean. They suggest that the AMO is a direct response of the ocean to atmospherically generated NAO variations and associated turbulent surface heat flux variations, combined with wind-evaporation-SST feedback in the tropics. However, this new perspective is challenged by recent analyses showing that ocean dynamics plays a central role in the AMO (Zhang et al. 2016; O'Reilly et al. 2016).

In this study we reexamine the connection between the NAO and Atlantic SST variability across a range of time scales using a combination of observational analyses and specifically designed climate model experiments. We show that ocean dynamics is critical to understanding the processes driving key aspects of the AMO in models and observations, especially in the subpolar gyre. AMO variability in the subtropics likely involves additional atmospheric processes, such as cloud feedback (Bellomo et al. 2015; Martin et al. 2014) or dust (Evan et al. 2009; Wang et al. 2012; Yuan et al. 2016; Brown et al. 2016).

2. Observational Data and Model Simulations

We use a combination of observational analyses and specifically designed numerical experiments.

2.1 Observational data

We use sea surface temperatures (SST) from ERSST(Smith et al. 2008) and an index of the NAO based on normalized station data (obtained from NCAR/UCAR Data Climate Guide at

https://climatedataguide.ucar.edu/climate-data/hurrell-north-atlantic-oscillation-nao-index-station-based) over the Dec-Mar (DJFM) period. We use both annual mean and winter (DJFM) mean SST and find comparable results, so that we only show results using annual mean SST.

2.2 Models

We use two climate models, with two variants of each model. The first model is GFDL CM2.1(Delworth et al. 2006), consisting of an atmospheric general circulation model coupled to an ocean general circulation model. The horizontal resolution of the atmosphere is approximately 200 km, with 24 vertical levels. The horizontal resolution of the ocean is approximately 1^{o}, with meridional refinement to 0.33^{o} in the deep Tropics. The model ocean has 50 levels in the vertical. We also use the FLOR model(Vecchi et al. 2014) which uses similar atmospheric physics as CM2.1 but with considerably higher spatial resolution in the atmosphere and land (approximately 50 km), with 32 vertical levels in the atmosphere. The ocean component of FLOR has the same spatial resolution as CM2.1, with similar physics. For each model (CM2.1 and FLOR) a variant is constructed (CM2.1_SLAB and FLOR_SLAB, respectively) in which the dynamic ocean component is replaced by a slab of fixed 50 m depth, with no interannual variations of ocean heat transport. In order for the slab models to have a realistic mean state and seasonal cycle of SST in the absence of resolved ocean heat transport, we add to the slab ocean model an additional heat flux adjustment term. The flux adjustments are calculated using preliminary separate simulations of the CM2.1_SLAB and FLOR_SLAB models in which model SST are restored (with a 5-day restoring time scale) to observed monthly SST over the period 1971-2012. The observed monthly SST are interpolated to daily values for the restoring runs. The time-mean of the restoring heat flux used in these simulations is then defined as the heat flux adjustment term (separate adjustment fields for the CM2.1_SLAB and FLOR_SLAB models). The heat flux adjustment term varies as a function of space and the seasonal cycle, but is constant from one year to

the next. The various simulations of the CM2.1_SLAB and FLOR_SLAB models are then conducted in which the heat flux adjustment terms are applied. Using these flux adjustments, the slab models have considerably reduced SST biases relative to the models with dynamic oceans.

We conduct several types of experiments with various sets of the available models (CM2.1, CM2.1_SLAB, FLOR, and FLOR_SLAB). The various experiments are listed in Table 1, and described below. With each model we conduct multi-century CONTROL simulations in which the atmospheric composition and radiative forcing is held fixed at either preindustrial (1860) or "modern" (1990) conditions. Using CM2.1, CM2.1_SLAB and FLOR we conduct experiments (called CM2.1_HIST, CM2.1_SLAB_HIST, and FLOR_HIST) in which estimates of the time-varying radiative forcing over the period 1861-2015 are applied to the model. We use ensembles to better define the response to radiative forcing. For CM2.1 and CM2.1_SLAB_HIST we use ten-member ensembles, whereas for FLOR_HIST we use five member ensembles. The ensemble members are started from widely separated points in their respective Control simulations. The response to radiative forcing is defined as the ensemble mean from the simulation with time-varying radiative forcing minus the ensemble mean from the corresponding sections of the Control simulations.

We also conduct simulations to explore the response of the system to an imposed NAO forcing. In these simulations we impose on the model ocean an additional pattern of surface heat flux anomalies that has the spatial pattern of the NAO. The pattern of the imposed heat flux anomalies is shown in Fig. 1a from Delworth and Zeng (2016). Specifically, after the atmosphere-ocean heat flux is calculated in the model, we add an extra term to the heat flux going into the model ocean. This extra heat flux has the spatial pattern of the NAO. We derive this pattern by computing a linear regression at each grid point between the time series of surface heat fluxes from the ECMWF-Interim reanalysis (Dee et al. 2011) and a time series of the observed NAO index. Both the NAO index and the surface

147 heat fluxes are time-means over the DJFM period. The surface heat flux includes the latent and
148 sensible terms, as well as shortwave and longwave radiative terms. The spatial pattern of the NAO-
149 related heat flux anomalies is fixed, but we modulate the amplitude of the flux forcing in time in
150 various ways as described below. We constrain the heat flux anomaly so that its' spatial integral is
151 zero. Therefore, the imposition of this anomaly pattern does not directly add heat to (or subtract heat
152 from) the climate system. This technique is similar to that employed in an earlier pioneering study
153 using an ocean-only model (Eden and Jung 2001), in contrast to the fully coupled model used here.

154 a. Idealized forcing experiments

155 In a first set of experiments we add the specified pattern of NAO-related heat flux forcing to the
156 ocean component of the CONTROL simulations for CM2.1, CM2.1_SLAB, and FLOR. The NAO flux
157 forcing is modulated in time by a sine wave with a 50-year period, whose amplitude corresponds to
158 one standard deviation of the observed NAO time series (identified in Table 1 as
159 CM2.1_Ctrl_NAO_50yr, CM2.1_SLAB_Ctrl_NAO_50yr, and FLOR_Ctrl_NAO_50yr). This 50-year
160 timescale is idealized, but is loosely based on the observed NAO variations over the 20th century,
161 which have substantial variability on multidecadal time scales (see, for example,
162 https://climatedataguide.ucar.edu/climate-data/hurrell-north-atlantic-oscillation-nao-index-station-
163 based). The simulations are 100 years long, with 10-member ensembles for CM2.1 and CM2.1_SLAB,
164 and 5-member ensembles for FLOR.

165 b. Realistic forcing experiments

166 In an additional set of experiments we add to the HIST simulations (CM2.1_HIST,
167 CM2.1_SLAB_HIST, and FLOR_HIST) the spatial pattern of the NAO heat flux, but multiplied each year
168 by the observed value of the NAO index over the period 1901-2014 for the CM2.1 and SM2.1 models,
169 and over the period 1951 to 2014 for the higher resolution (and more computationally expensive)

FLOR model. These experiments are identified in Table 1 as CM2.1_HIST_NAO, CM2.1_SLAB_HIST_NAO, and FLOR_HIST_NAO. Differences between the experiments with NAO forcing and their counterparts without NAO forcing (for example, CM2.1_HIST_NAO minus CM2.1_HIST) show the climatic impact of the NAO forcing added to the model ocean. This yields some assessment of the contribution of NAO variations to observed climate variations in terms of the impact of the NAO on the ocean and subsequent feedback to the atmosphere. In these experiments there is no anomalous flux forcing applied to the atmosphere – the anomalous NAO fluxes are only directly felt by the ocean. The observed NAO index is taken from https://climatedataguide.ucar.edu/climate-data/hurrell-north-atlantic-oscillation-nao-index-station-based. The heat flux anomalies are only applied over the Dec-Mar period. We use ensembles to better estimate the response to the NAO (10 members for CM2.1_HIST_NAO and CM2.1_SLAB_HIST_NAO, and 5 members for FLOR_HIST_NAO).

The simulations with dynamic oceans have been previously analyzed and published in (Delworth and Zeng 2016) and (Delworth et al. 2016), while the simulations with slab oceans have not previously been analyzed.

We note that the model computes its own internal NAO variability, in addition to the imposed NAO forcing. This creates spread among the ensemble members in simulating the model response to the NAO forcing, since the model ocean responds both to the imposed NAO forcing and the internally generated NAO forcing. We evaluated the spread of the NAO by resampling the Control simulations of each model. Based on these analyses (see also Methods section of Delworth et al., 2016) we conclude that the NAO computed in each model is an important source of noise and ensemble spread, but that the NAO forced signal is still able to emerge from this noise when the NAO forcing is of sufficiently large amplitude, as is the case for the primary multidecadal swings of the NAO in the observational record.

3. Observed relationship between NAO and North Atlantic SST

We first examine the relationship between the NAO and SST in observations as a function of time scale. We filter the observed time series for the NAO and SST to retain either time scales shorter than 10 years ("High Pass filtered", or "HP") or longer than 10 years ("Low Pass filtered", or "LP), using a finite impulse response filter with 10 weights (Bloomfield 1976). We calculate the lagged correlations between the time series of annual mean SST at each grid point and the NAO time series for both the HP and LP data over the period 1861-2014. More specifically, a correlation at lag 0 refers to the correlation of the NAO index for the period of December (year 0) through March (year 1) with annual mean SST for January through December of year 1. As discussed in the Appendix, statistical significance was estimated using a Monte Carlo resampling technique. We show results in which the time series were not detrended prior to the analysis. When a linear trend is removed prior to the analyses, we find results that are generally similar to those shown below, with somewhat larger amplitudes.

At short time scales (Fig 1a) the largest amplitude correlations occur in the year immediately after the NAO maximum (defined as Lag 0), and correspond to a tripole pattern, with negative values in the subpolar gyre and tropical North Atlantic, and positive values in middle latitudes. This is consistent with atmospheric surface flux forcing of the ocean mixed layer, as shown by many past studies (Cayan 1992; Battisti et al. 1995). Correlation coefficients at other lags are considerably smaller.

We show the LP results in Fig. 1b. There is a tripole-like pattern for small lags, but the largest correlations occur at much larger lags. Positive correlations, covering most of the North Atlantic,

reach their maximum 15-30 years after the NAO maximum. This decadally-lagged relationship is distinctly different than the direct surface flux forcing of the mixed layer shown for the HP analyses.

We also note that there are significant negative correlations when SST leads the NAO by a decade or two. We present analyses in sections 4.2 and 4.4 to suggest that these negative correlations in fact represent a response to a preceding negative phase of the NAO, just as the positive correlations at a lag of one to two decades represent a response to a positive phase of the NAO. Underlying these relationships is the fact that the NAO has substantial multidecadal variability in the (relatively short) observed record.

The spatial patterns of the correlation coefficients are shown in Figure 2. The pattern with maximum correlations using HP data is shown in Fig. 2a, occurring for annual mean SST immediately following the DJFM NAO, and is a clear tripole. Shown in Fig 2b are the correlations using LP data when SST lags the NAO by 15 years. The pattern is of largely uniform sign across the basin, resembling the observed AMO (Sutton and Hodson 2005), and is distinctly different than the tripole structure. We show in Figs 2c-2h the temporal evolution of the LP SST signal with respect to the NAO. For periods before the NAO maximum, SST anomalies are generally negative over the North Atlantic. A few years after the NAO reaches its maximum, positive SST anomalies develop in the central North Atlantic. This region expands northward and equatorward, encompassing most of the North Atlantic by 10-15 years after the NAO maximum, with the largest signal in the subpolar North Atlantic. The initial appearance of the positive SST anomaly in the central North Atlantic and its subsequent apparent propagation appear consistent with a significant role for ocean dynamics, but this is difficult to explore solely from observational analyses. We therefore turn to modeling experiments to explore further the relationship between the NAO and Atlantic decadal SST variability.

4. Simulated relationship between NAO and North Atlantic SST

In this section we explore the relationship between the NAO and North Atlantic interannual to multidecadal SST variability in a suite of climate model simulations.

4.1 Control simulations

We first explore this relationship in a set of Control simulations. We show in Figure 3 the zonal means of the correlation coefficients between annual mean SST anomalies and the DJFM NAO as a function of lag. We show results for HP and LP filtered data. We also show results for models using either a slab ocean (left column) or a dynamic ocean (right column). For all results with models using a slab ocean model (ie., no ocean dynamics), the largest correlations are at Lag 0 (HP data) or are centered around Lag 0 (LP data), with no substantial correlations at lags greater than +/- 5 years. This is consistent with observational analyses at short time scales (compares Figs. 3a and 3c to Fig. 1a), but inconsistent with observations at long time scales (compare Figs. 3b and 3d to Fig. 1b). When using a dynamic ocean (right column in Figure 3), the models are similar to observations at short time scales (Figs. 3e and 3g), with maximum correlations at lag one, and the spatial structure is consistent with the tripole pattern. The model correlations are somewhat weaker than those from observational analyses. This difference could be related to sampling uncertainty with far fewer points in the observational record or to incorrectly represented processes in the models.

At long time scales the models with dynamic oceans show the maximum correlation lagged a decade or so after the NAO maximum (Figs. 3f and 3h). This lag is shorter in the models than in observations (Fig. 1b). This phase lag between the NAO and SST anomalies at long time scales, similar to observations, only appears when ocean dynamics are considered.

263 We show in Figure 4 the spatial pattern of the correlations between SST and the NAO at the lag
264 corresponding to the largest correlations based on Fig. 3. For all of the cases using HP data (left
265 column) the maximum correlation occurs for the year immediately after the NAO maximum, and
266 resembles the tripole pattern. This was true regardless of whether the model used a slab ocean(Figs.
267 4a and 4c) or a dynamic ocean (Figs. 4b and 4d). In contrast, there are differing behaviors using LP
268 data (right column). For the models with slab oceans (Figs. 4e and 4g) the maximum correlation is
269 also at the year immediately following the NAO maximum, and the spatial correlation is the familiar
270 tripole pattern. In contrast, for models with dynamic oceans (Figs. 4f and 4h) the maximum
271 correlation occurs approximately 7-10 years after the NAO maximum, and is characterized by a
272 monopole, AMO-like pattern over the North Atlantic, somewhat resembling the observations (Figure
273 1b), although with a smaller than observed amplitude in the tropical North Atlantic. Again, this points
274 to a fundamental role of ocean dynamics for decadal scale Atlantic SST variability, especially in the
275 subpolar gyre region.
276
277 **4.2 Simulations with periodic NAO forcing**
278
279 We further explore the relationship between the NAO and Atlantic SST anomalies by analyzing
280 simulations using a 50 year idealized NAO forcing using the CM2.1, CM2.1_SLAB, and FLOR models.
281 Normalized time series of the idealized NAO variability and associated heat flux forcing in the
282 subpolar gyre are shown in Fig. 5a. Positive NAO values are associated with strengthened westerly
283 winds over the subpolar North Atlantic. These in turn lead to negative heat flux anomalies, where a
284 negative heat flux anomaly denotes enhanced ocean to atmosphere heat flux.
285 For the model with a slab ocean (Fig. 5b) the zonal mean SST response to the 50 year NAO
286 forcing is largely in phase with the NAO flux forcing (Fig. 5a), but with a small lag. Here, "in phase"

means that negative SST anomalies in the subpolar gyre occur at the same time as a positive phase of the NAO (with enhanced ocean to atmosphere heat flux which leads to cooling of the ocean mixed layer). The small phase lag between the maximum NAO and the coolest SSTs represents the finite heat capacity of the 50 meter mixed layer ocean, such that the mixed layer temperature lags the forcing somewhat. The above results show that the response is dominated by the direct effects of the turbulent surface heat fluxes on the upper ocean.

In contrast, for the two models with dynamic oceans (Figs. 5c and 5d), positive SST anomalies over the subpolar gyre lag the NAO by 5-10 years. This behavior reflects the role of ocean dynamics, and shows a fundamentally different relationship between the NAO and Atlantic SSTs at middle and high latitudes in the presence of a dynamic ocean (Bjerknes 1964; Eden and Jung 2001). With a dynamic ocean the dominant response on long time scales (ie, to the 50 year forcing) is not the direct flux forced tripole pattern, but a lagged monopole pattern that arises due to a lagged response of the AMOC (Delworth and Zeng 2016). In the models with dynamic oceans the NAO forcing extracts heat from the subpolar gyre, leading to an increase of upper-ocean density, oceanic convection, deepwater formation, and the AMOC. The AMOC response to the 50 year NAO forcing is shown in Figs. 5e and 5f. The periodic NAO forcing generates a periodic AMOC variability, with the AMOC lagging the forcing by a few years. The positive (negative) AMOC anomalies induce stronger (weaker) than normal poleward heat transport in the North Atlantic (Fig. 5g), leading to widespread warming (cooling) in the North Atlantic. The accumulating heat in the subpolar gyre associated with enhanced ocean heat transport leads to a lag of several years between the maximum AMOC anomaly and the maximum SST anomaly.

We further illustrate in Fig. 6 the relationships on decadal scales between the NAO and large-scale simulated SST by computing lead-lag correlations between the simulated SST response in the 50 year NAO forcing experiments and the imposed NAO anomaly, similar to Figs 1 and 3. For the slab

ocean case (Fig. 6a), the largest negative correlations occur at a small lag with respect to the NAO. This again shows that the slab ocean response is dominated by the direct impact of the anomalous surface heat flux forcing, with a small lag due to the thermal capacity of the ocean mixed layer.

For both the CM2.1 and FLOR simulations with dynamic ocean, the maximum positive correlations lag the imposed NAO forcing by approximately 10 years, demonstrating that the NAO forcing induces a warming of the North Atlantic with a decadal-scale lag. We note that there are also negative correlations for periods preceding the NAO forcing, reminiscent of the observational analyses in Fig. 1b. The North Atlantic SST responds to a positive phase of the NAO with a delayed warming as a result of a decadal-scale adjustment of the AMOC to the NAO forcing. A similar process occurs in response to a negative NAO. The negative correlations for negative lags indicate a weakening of the AMOC in response to the negative phase of the NAO which precedes the positive phase of the NAO by 25 years in these idealized experiments. These results are of relevance for interpreting the observational analyses in Fig. 1b. During the instrumental record the observed NAO has been characterized by substantial multidecadal variability (see https://climatedataguide.ucar.edu/climate-data/hurrell-north-atlantic-oscillation-nao-index-station-based), with positive NAO phases in the early and late 20th century, and negative phases in the late 19th and mid 20th centuries. The model results shown in Fig. 6 suggest that the observed negative correlations in Figure 1b for negative lags may be related to multidecadal variability in the observed NAO. Just as for the model results in Fig. 6, the observed negative correlations at negative lags may be the lagged response to a negative phase of the NAO, which precedes the positive phase of the NAO by several decades in both the observations and the idealized simulations. This is explored further in section 4.4.

4.3 Results from other models

In order to provide some assessment of the robustness of the NAO relationship with simulated North Atlantic decadal SST variability, we repeat the correlation analyses shown in Fig. 3 using a variety of control simulations from the CMIP5 archive. The results are shown in Fig. 7, and indicate that many (but not all) models have a similar relationship between the NAO and decadal scale North Atlantic SST variability. Somewhat similar behavior is seen in ACCESS1-0, NorESM1-M, CCSM4, MPI-ESM-LR, MPI-ESM-MR, CSIRO-Mk3-6-0, IPSL-CM5A-LR and IPSL-CM5-MR. Rather different behavior, however, is seen in HadGEM2C-CC and MIROC-ESM-CHEM. The details can vary widely, however, and may be sensitive to a number of factors, including the spatial structure of the model simulated NAO, the climatological ocean circulation, regions of simulated deep water formation, and the overall structure of biases in the model simulation. The overall results are sufficiently similar to suggest that the results shown in Fig. 3 are not unique to the GFDL models, but substantial uncertainty remains.

4.4 Simulations of 20th and 21st centuries

We next analyze the output from experiments using a realistic time history of NAO forcing to provide a perspective on the relationship between the NAO and Atlantic decadal SST variations in the observed record. For example, differences between CM2.1_HIST_NAO and CM2.1_HIST reflect the impact of the observed NAO variations on the climate system over the period 1901-2014. For each model we use ensembles to improve the signal to noise ratio (ten-member ensembles for CM2.1 and CM2.1_SLAB, 5-member ensembles for FLOR). We note that the FLOR simulations only go from 1951-2015 due to the greater computational expense of the FLOR model.

We show in Figure 8a the time series of the observed NAO, and in Figure 8b the time series of the imposed surface heat flux anomalies over the Labrador Sea that are associated with the observed

NAO anomalies (these are the extra fluxes added in the "NAO" experiments). The heat flux anomalies are only applied over December-March, with zero anomalies over the rest of the year; the time series shown in Figure 8a is expressed here as annual means. The positive heat flux anomalies in the 1960s and 1970s are consistent with negative NAO anomalies in that time period, resulting in reduced ocean to atmosphere heat fluxes (appearing here as positive heat flux anomalies into the ocean). We show in Figure 8c the time series of annual mean observed SST anomalies averaged over the domain 60^0W-20^0W, and 30^0N-65^0N. This clearly shows multidecadal warming and cooling associated with the AMO. In Figs. 8d and 8e we show the simulated response to the observed NAO flux anomalies using CM2.1 and FLOR, respectively, averaged over the same domain as the observations. Both models capture the essence of the observed AMO signal in the extratropical North Atlantic, with negative (positive) SST anomalies appearing a decade or so after the NAO minimum (maximum). In both cases the SST response is associated with a lagged response of the AMOC to the NAO fluxes (see Fig. 1 in Delworth et al., 2016), thereby altering oceanic heat transport and creating basin scale monopole SST anomaly patterns. We show in Fig. 8f the results using CM2.1_SLAB. When we replace the dynamic ocean of CM2.1 with the 50 m slab ocean, the response to exactly the same set of NAO surface heat flux anomalies is substantially different. In the slab model negative SST anomalies are a direct response to a positive phase of the NAO. Therefore, while both observations and the models with the dynamic ocean show widespread warming in the 1990s and 2000s (a delayed response to the positive phase of the NAO), the slab model shows pronounced negative SST anomalies in the 1990s and 2000s, opposite to the observed signal. Therefore, we conclude that ocean dynamics are an essential part of the processes governing AMO-like SST variations over the subpolar gyre in the models, and also in observations.

The observations (Fig. 8c) show a rapid warming in the 1990s in the North Atlantic. We show the spatial pattern of that warming, relative to the cool period of the 1970s and early 1980s, in Figure 9a. The observations show warming extending from the subpolar to the subtropical North Atlantic. We show the degree to which each of the models is able to simulate that warming in response to historical radiative forcing and/or NAO flux forcing. The left column shows the SST response due to radiative forcing alone (HIST simulations), the middle column shows the SST response due to both radiative forcing and the imposed NAO flux anomalies (HIST_NAO simulations), and the right column shows the impact of only the NAO flux forcing, estimated as the HIST_NAO simulations minus the HIST simulations. The left column shows substantial warming due purely to radiative forcing, primarily equatorward of 40^{o}N for the models with dynamic ocean. The model with a slab ocean shows very large warming extending poleward of 70^{o}N. The areal mean warming with the slab ocean model is 2.5 times larger than observed, likely related to the small effective ocean heat capacity of the 50 m slab ocean..

The middle column shows the results when including the NAO forcing in addition to the radiative forcing. While there is very little change (relative to HIST) for the model with a slab ocean, the warming for CM2.1 and FLOR extends much further north, into the Nordic Seas. The impact of the NAO is isolated in the third column by substracting the HIST results from the HIST_NAO results. This shows that for the models with dynamic oceans the extratropical warming (from the 1970s to the 1990s) has a very significant contribution from NAO forced ocean circulation changes. In contrast, the slab ocean shows little additional impact from the NAO forcing.

The CM2.1_HIST_NAO simulation extends from 1901 to 2014, and the CM2.1_HIST covers the period 1861 to 2014. We can therefore compute lead-lag correlations between the observed NAO and SST in each of these two simulations, similar to Figure 1. These are shown in Figure 10 for the

CM2.1_HIST_NAO simulations (top panel) and the CM2.1_HIST simulations (bottom panel). A number of features are present. First, we note that the CM2.1_HIST_NAO simulations have weak negative correlations when SST leads the NAO by approximately 20 years, somewhat similar to the observations in Fig. 1b. As discussed with regard to Figure 6, one interpretation of this is that these negative correlations reflect a weakening of the AMOC (and hence negative SST anomalies) in response to a previous negative phase of the NAO. We note that the observed NAO in the 20th century is characterized by clear multidecadal variability. When we impose this NAO forcing on the model ocean, as in CM2.1_HIST_NAO, we reproduce some aspects of the negative correlations between SST and the NAO when SST leads the NAO. In contrast, this negative correlation is absent in the bottom panel in which there are no imposed NAO anomalies. This provide support to the idea that the negative correlations that occur when SST leads the NAO by a decade or two are a result of the weakened AMOC in response to a prior negative phase of the NAO.

We also note that there are positive correlations when SST lags the NAO by a decade or so in the CM2.1_HIST_NAO simulations, as we have seen previously. These have largest values in the subpolar gyre, consistent with our previous analyses. We also note modest positive correlations in the NAO_HIST simulations. This relationship is weak and likely insignificant, and could result from some similar aspects of long term trends in the observed NAO and the response of the North Atlantic ocean to radiative forcing changes.

In summary, the above results suggest that that multidecadal variations of North Atlantic SST are a combination of the response to changing radiative forcing and to multidecadal ocean circulation changes induced by multidecadal NAO variations. For these models with a dynamic ocean, the NAO driven changes have largest amplitude in the middle and higher latitudes of the North Atlantic, whereas at lower latitudes the relative impact of radiative forcing is larger. This decomposition

occurs in models for which NAO driven AMOC variability results in a much smaller response in the tropical North Atlantic than in the subpolar North Atlantic. It is possible that this small tropical response is related to deficiencies in model processes, such as cloud or dust feedbacks. If that were the case the potential importance of NAO driven AMOC and ocean heat transport variability for tropical North Atlantic climate variability could be larger.

We note that our results provide some contrast to a recent study on this topic (Clement et al. 2015), in which it was concluded that the AMO in models with a dynamic ocean is mainly due to the direct influence of NAO variations on the heat budget of the ocean mixed layer, combined with wind-evaporation-SST feedback in the tropics. The pattern of surface flux forcing employed in the current study is similar in character to the dominant pattern of coupled ocean-atmosphere variability in their study that resembled the NAO. Nevertheless our results point to the importance of ocean dynamics through a delayed response of the AMOC and resultant changes to basin-scale meridional oceanic heat transport, especially for the subpolar gyre of the North Atlantic.

5. Summary and Discussion

Using observations and models we have examined the relationship between the North Atlantic Oscillation (NAO) and Atlantic decadal SST variations. Consistent with many previous studies, on short time scales NAO related surface heat flux anomalies drive a tripole pattern of SST anomalies in the Atlantic. On decadal and longer time scales there is a lagged response of the ocean to the NAO fluxes, with the AMOC playing a prime role in modulating meridional oceanic heat transport and generating an AMO-like SST response. A prolonged positive phase of the NAO enhances the AMOC after a decadal-scale delay.

We further show that ocean dynamics are crucial to the relationship on decadal scales. We use simulations with slab oceans to show that without ocean dynamics the relationship of Atlantic decadal SST anomalies to the NAO is nearly opposite to that in models with ocean dynamics, primarily over the subpolar gyre, and different from observations. Further, the NAO-SST relationship in models with ocean dynamics bears a considerable resemblance in middle and higher latitudes of the North Atlantic to the relationship diagnosed from observations.

In the models used for the present study the phase lag between the NAO and Atlantic decadal SST anomalies is shorter than that seen in observations. It is difficult to properly characterize this relationship given the short observational record. However, this difference is consistent with the relatively short timescale of AMOC variability in these models (20-30 years) relative to the timescale of the observed AMO. The response of models to NAO variability is a key aspect of Atlantic decadal variability, and is an important component underlying the physical basis for decadal prediction. It is important to stress that atmospheric circulation variability in addition to the NAO may be very important for driving Atlantic ocean variability (Barrier et al. 2014).

The resemblance of the models to observations is weaker over the subtropical North Atlantic than over the subpolar North Atlantic. This discrepancy highlights the importance of additional atmospheric processes, some not well captured in many current models, which influence decadal-scale variability over the North Atlantic. The impact of time-varying anthropogenic aerosols (Booth et al. 2012), dust emissions from the African continent (Evan et al. 2009) , as well as cloud feedback and circulation linkages (Martin et al. 2014), may be critical for Atlantic variability. Variations of the North Atlantic Oscillation are one mechanism contributing to the observed decadal-scale variability of the North Atlantic through its impact on the AMOC, but a more complete understanding of observed Atlantic decadal variability needs to properly account for all of the important additional factors. This

is particularly important since many of the large-scale tropical climatic impacts associated with Atlantic decadal SST variability are influenced most strongly by the SST signal in the tropical North Atlantic. It is critical that models improve their ability to faithfully represent all of these important processes to allow us a better quantitative assessment of the processes governing observed Atlantic changes. Such improved understanding would then lend increased confidence to our predictions of future changes.

Acknowledgements

The authors are grateful to Dr. Yohan-Ruprich Robert and Dr. Honghai Zhang for very valuable comments on an earlier version of this manuscript, as well as three anonymous reviewers who provided extremely insightful and valuable feedback and suggestions. The NOAA_ERSST_V3 data was downloaded from NOAA/OAR/ESRL PSD, Boulder, Colorado, USA, from their Web site at http://www.esrl.noaa.gov/psd/. Observed NAO data was downloaded from https://climatedataguide.ucar.edu/climate-data/hurrell-north-atlantic-oscillation-nao-index-station-based. We acknowledge the World Climate Research Programme's Working Group on Coupled Modelling, which is responsible for CMIP, and we thank the climate modeling groups (models shown in Figure 7) for producing and making available their model output. For CMIP the U.S. Department of Energy's Program for Climate Model Diagnosis and Intercomparison provides coordinating support and led development of software infrastructure in partnership with the Global Organization for Earth System Science Portals. The work of T. Delworth, G. Vecchi, F. Zeng and R. Zhang is supported as a base activity of NOAA's Geophysical Fluid Dynamics Laboratory. X. Yang is supported through UCAR under block funding from NOAA/GFDL. L. Zhang is supported through Princeton University under block funding from NOAA/GFDL.

496

Appendix – Statistical testing for Figures 1, 3, 6, and 10

Figure 1 is constructed by first computing the linear correlation coefficients between the observed NAO index and the time series of observed SST at each grid point in the North Atlantic. Prior to the analysis the NAO and SST data were subject to either a low-pass (longer then ten years) or high-pass (shorter than ten years) filter. The correlation analysis is performed for various leads and lags. The correlation values are then zonally averaged over the longitudinal span 60^{o}W-20^{o}W, and then plotted as a function of lag and latitude. The analysis using high-pass filtered data is shown in Figure 1a, and using low-pass filtered data in Fig. 1b.

We assess the significance of these plotted values using the following resampling strategy. A similar strategy is used for both Fig. 1a and 1b. We use observed time series of both the NAO and SST over the period 1864-2014 (151 years total), using the NDJF seasonal mean for the NAO and annual means for SST. In our resampling strategy we first choose a year at random between 1864 and 2014. We then create a new "shuffled" NAO time series. The first part of this new "shuffled" time series consists of the original NAO time series starting from the chosen random year, continuing to 2014; the second part of the time series uses the original NAO data from 1864 to the year before the randomly chosen year. For example, if the random year were 1922, then the shuffled NAO time series would consist of the original NAO time series value from 1922-2014, followed immediately by the original NAO time series from 1864-1921. This "shuffled" time series has many of the same temporal properties as the original NAO time series, but the starting year is redefined. We then choose a second random year to do a similar "reshuffling" process to the time series of observed annual mean SST, using the same random year to perform the reshuffling for SST at each grid point. Thus, the NAO and SST time series have been independently reshuffled. We now compute the linear correlation coefficients between the reshuffled NAO and SST time series at each grid point. We then compute the

zonal average of the correlations over the range 60°W to 20°W. We repeat the above process 10,000 times to form a distribution for each latitude and lag of the zonal mean correlations between randomly reshuffled NAO and SST time series. Threshold values in those distributions are found such that 10% of the distribution has values smaller than the first threshold, and 10% of the distribution has values larger than the second threshold. Hatching is placed in Figure 1 on those grid points where the correlation values are between the two thresholds. We note that when computing lagged correlations the number of points in the correlation calculation is reduced by the lag in use (ie, for lag 10 there are 10 fewer points in the correlation calculations). We therefore compute a separate distribution for each length of time series ranging from 151 (original time series) to 131 (lag 20), and use the appropriate distribution for each lag to calculate the threshold values.

By chance we would expect 80% of the points to have hatching and 20% of the points to have no hatching. For the area poleward of 30°N (where we have an a priori expectation that on long time scales the NAO will lead SST), we calculate that 40% of the points have no hatching in Fig. 1b, which is substantially larger than the 20% one would expect from chance. We therefore conclude that there is a statistically meaningful correlation between the NAO and SSTs at long time scales, especially in the mid and higher latitudes of the North Atlantic.

Figure 3 is constructed in a similar fashion to Figure 1, but using model output from three separate Control simulations. At each lag, the correlations (calculated between the model's SST and NAO) are zonally averaged over 60°W to 20°W in the North Atlantic for each latitude band. We place stippling over latitudes and lags that are not statistically significant. This assessment was based on the following: at each grid point, and for each lag, we use a Student's t test to assess whether the correlation coefficient was significantly different from zero at the 90% confidence level for that particular lag. We then evaluate, for each lag and latitude, how many points in the zonal band from

543 60°W to 20°W are significant by that metric. Separately, we evaluate the number of grid points that
544 would be expected to pass such a significance test by chance at various levels of confidence. The
545 regions without (with) stippling indicate areas where this value of the zonal mean correlation has less
546 than (greater than) a 10% chance of occurring by chance. A similar method was used to assess
547 statistical significance in **Figures 6 and 10**, with the exception that for Figure 10 the regions without
548 (with) stippling indicate areas where this value of the zonal mean correlation has less than (greater
549 than) a 20% chance of occurring by chance. We have performed these tests with varying confidence
550 levels and estimates of degrees of freedom, but the essential results are largely robust.
551
552 **References**
553
554 Barrier, N., C. Cassou, J. Deshayes, and A.-M. Treguier, 2014: Response of North Atlantic Ocean
555 Circulation to Atmospheric Weather Regimes. *J. Phys. Oceanogr.*, **44**, 179–201,
556 doi:10.1175/JPO-D-12-0217.1.

557 Battisti, D. S., U. S. Bhatt, and M. Alexander, 1995: A modeling study of the interannual variability in
558 the wintertime North Atlantic ocean. *J. Clim.*, **8**, 3067–3083.

559 Bellomo, K., A. C. Clement, T. Mauritsen, G. Rädel, and B. Stevens, 2015: The Influence of Cloud
560 Feedbacks on Equatorial Atlantic Variability. *J. Clim.*, **28**, 2725–2744, doi:10.1175/JCLI-D-14-
561 00495.1.

562 Bjerknes, J., 1964: Atlantic Air-Sea Interaction. *Advancs in Geophysics.*, Vol. 10 of *Advances in*
563 *Geophysics.*, Academic Press, Inc., New York, USA, 1–82.

564 Bloomfield, P., 1976: *Fourier Analysis of Time Series: An Introuction.* John Wiley and Sons, 258 pp.

565 Booth, B. B. B., N. J. Dunstone, P. R. Halloran, T. Andrews, and N. Bellouin, 2012: Aerosols implicated as
566 a prime driver of twentieth-century North Atlantic climate variability. *Nature*, **484**, 228–232,
567 doi:10.1038/nature10946.

568 Brown, P. T., M. S. Lozier, R. Zhang, and W. Li, 2016: The necessity of cloud feedback for a basin-scale
569 Atlantic Multidecadal Oscillation: Cloud feedback causes basin-scale AMO. *Geophys. Res. Lett.*,
570 doi:10.1002/2016GL068303. http://doi.wiley.com/10.1002/2016GL068303 (Accessed May 3,
571 2016).

572 Cayan, D. R., 1992: Latent and sensible heat flux anomalies over the Northern Oceans: Dirving the Sea
573 Surface Temperature. *J. Phys. Oceanogr.*, **22**, 859–881.

574 Chylek, P., C. K. Folland, G. Lesins, M. K. Dubey, and M. Wang, 2009: Arctic air temperature change
575 amplification and the Atlantic Multidecadal Oscillation. *Geophys. Res. Lett.*, **36**,
576 doi:10.1029/2009GL038777. http://doi.wiley.com/10.1029/2009GL038777 (Accessed May
577 29, 2015).

578 ——, M. K. Dubey, G. Lesins, J. Li, and N. Hengartner, 2014: Imprint of the Atlantic multi-decadal
579 oscillation and Pacific decadal oscillation on southwestern US climate: past, present, and
580 future. *Clim. Dyn.*, **43**, 119–129, doi:10.1007/s00382-013-1933-3.

581 Clement, A., K. Bellomo, L. Murphy, M. Cane, T. Mauritsen, G. Radel, and B. Stevens, 2015: The Atlantic
582 Multidecadal Oscillation without a role for ocean circulation. *Science*, **350**,
583 doi:10.1126/science.aab3980.

584 Daly, A., 1978: The response of North Atlantic sea surface temperature to atmospheric forcing
585 processes. *Q. J. R. Meteorol. Soc.*, **104**, 363–382.

586 Danabasoglu, G., S. G. Yeager, Y.-O. Kwon, J. J. Tribbia, A. S. Phillips, and J. W. Hurrell, 2012: Variability
587 of the Atlantic Meridional Overturning Circulation in CCSM4. *J. Clim.*, **25**, 5153–5172,
588 doi:10.1175/JCLI-D-11-00463.1.

589 Dee, D. P., and Coauthors, 2011: The ERA-Interim reanalysis: configuration and performance of the
590 data assimilation system. *Q. J. R. Meteorol. Soc.*, **137**, 553–597, doi:10.1002/qj.828.

591 Delworth, T. L., and F. Zeng, 2016: The impact of the North Atlantic Oscillation on climate through its
592 influence on the Atlantic Meridional Overturning Circulation. *J. Clim.*, **Accepted**.

593 ——, S. Manabe, and R. J. Stouffer, 1993: Interdecadal variations of the Thermohaline Circulation in a
594 Coupled Ocean-Atmosphere Model. *J. Clim.*, **6**, 1993–2011.

595 ——, and Coauthors, 2006: GFDL's CM2 global coupled climate models. Part I: Formulation and
596 simulation characteristics. *J. Clim.*, **19**.
597 http://search.ebscohost.com/login.aspx?direct=true&profile=ehost&scope=site&authtype=cra
598 wler&jrnl=08948755&AN=20383623&h=2sJeKz%2FGMqTzVHHQBKa2e%2BZ7toLSVvgfC3dF
599 fhx4PsbzDMGvlGmfQy1KkV6BphqH64hJN1LDt15ifiVxKq%2BWdA%3D%3D&crl=c (Accessed
600 April 2, 2014).

601 ——, F. Zeng, G. A. Vecchi, X. Yang, L. Zhang, and R. Zhang, 2016: The North Atlantic Oscillation as a
602 driver of rapid climate change in the Northern Hemisphere. *Nat. Geosci.*, **9**, 509–512,
603 doi:10.1038/ngeo2738.

604 Eden, C., and T. Jung, 2001: North Atlantic interdecadal variability: oceanic response to the North
605 Atlantic Oscillation (1865-1997). *J. Clim.*, **14**, 676–691.

606 Enfield, D. B., A. M. Mestas-Nuñez, and P. J. Trimble, 2001: The Atlantic multidecadal oscillation and its
607 relation to rainfall and river flows in the continental US. *Geophys. Res. Lett.*, **28**, 2077–2080.

608 Evan, A. T., D. J. Vimont, A. K. Heidinger, J. P. Kossin, and R. Bennartz, 2009: The Role of Aerosols in the
609 Evolution of Tropical North Atlantic Ocean Temperature Anomalies. *Science*, **324**, 778–781,
610 doi:10.1126/science.1167404.

611 Folland, C. K., T. N. Palmer, and D. E. Parker, 1986: Sahel rainfall and worldwide sea temperatures,
612 1901-85. *Nature*, **320**, 602–607.

613 Grossmann, I., and P. J. Klotzbach, 2009: A review of North Atlantic modes of natural variability and
614 their driving mechanisms. *J. Geophys. Res.*, **114**, doi:10.1029/2009JD012728.
615 http://doi.wiley.com/10.1029/2009JD012728 (Accessed April 6, 2016).

616 Gulev, S. K., M. Latif, N. Keenlyside, W. Park, and K. P. Koltermann, 2013: North Atlantic Ocean control
617 on surface heat flux on multidecadal timescales. *Nature*, **499**, 464–467,
618 doi:10.1038/nature12268.

619 Hu, Q., and M. C. Veres, 2016: Atmospheric Responses to North Atlantic SST Anomalies in Idealized
620 Experiments. Part II: North American Precipitation. *J. Clim.*, **29**, 659–671, doi:10.1175/JCLI-D-
621 14-00751.1.

622 Keenlyside, N., Jin Ba, Jennifer Mecking, Nour-Eddine Omrani, Mojib Latif, Rong Zhang, and Rym
623 Msadek, 2013: North Atlantic Multi-Decadal Variability ? Mechanisms and Predictability.

624 *Climate Change: Multidecadal and Beyond*, Vol. Volume 6 of *World Scientific Series on Asia-*
625 *Pacific Weather and Climate*, WORLD SCIENTIFIC, 141–157
626 http://dx.doi.org/10.1142/9789814579933_0009 (Accessed May 3, 2016).

627 Kerr, R. A., 2000: A North Atlantic Climate Pacemaker for the Centuries. *Science*, **288**, 1984–1985,
628 doi:10.1126/science.288.5473.1984.

629 Knight, J. R., R. Allan, C. K. Folland, M. Vellinga, and M. E. Mann, 2005: A signature of persistent natural
630 thermohaline circulation cycles in observed climate. *Geophys. Res. Lett.*, **32**,
631 doi:10.1029/2005GL024233. http://doi.wiley.com/10.1029/2005GL024233 (Accessed April
632 28, 2015).

633 ——, C. K. Folland, and A. A. Scaife, 2006: Climate impacts of the Atlantic Multidecadal Oscillation.
634 *Geophys. Res. Lett.*, **33**, doi:10.1029/2006GL026242.
635 http://doi.wiley.com/10.1029/2006GL026242 (Accessed September 21, 2016).

636 Mahajan, S., R. Zhang, and T. L. Delworth, 2011: Impact of the Atlantic Meridional Overturning
637 Circulation (AMOC) on Arctic Surface Air Temperature and Sea Ice Variability. *J. Clim.*, **24**,
638 6573–6581, doi:10.1175/2011JCLI4002.1.

639 Martin, E. R., C. Thorncroft, and B. B. B. Booth, 2014: The Multidecadal Atlantic SST—Sahel Rainfall
640 Teleconnection in CMIP5 Simulations. *J. Clim.*, **27**, 784–806, doi:10.1175/JCLI-D-13-00242.1.

641 Nigam, S., B. Guan, and A. Ruiz-Barradas, 2011: Key role of the Atlantic Multidecadal Oscillation in
642 20th century drought and wet periods over the Great Plains: AMO'S ROLE IN GREAT PLAINS
643 DROUGHTS. *Geophys. Res. Lett.*, **38**, n/a – n/a, doi:10.1029/2011GL048650.

O'Reilly, C. H., M. Huber, T. Woollings, and L. Zanna, 2016: The signature of low-frequency oceanic forcing in the Atlantic Multidecadal Oscillation: LOW-FREQUENCY OCEANIC FORCING OF THE AMO. *Geophys. Res. Lett.*, **43**, 2810–2818, doi:10.1002/2016GL067925.

Smith, T. M., R. W. Reynolds, T. C. Peterson, and J. Lawrimore, 2008: Improvements to NOAA's Historical Merged Land–Ocean Surface Temperature Analysis (1880–2006). *J. Clim.*, **21**, 2283–2296, doi:10.1175/2007JCLI2100.1.

Sutton, R., and D. Hodson, 2005: Atlantic Ocean Forcing of North American and European Summer Climate. *Science*, **309**, 115–118.

Sutton, R. T., and B. Dong, 2012: Atlantic Ocean influence on a shift in European climate in the 1990s. *Nat. Geosci.*, **5**, 788–792, doi:10.1038/ngeo1595.

Vecchi, G. A., and Coauthors, 2014: On the Seasonal Forecasting of Regional Tropical Cyclone Activity. *J. Clim.*, **27**, 7994–8016, doi:10.1175/JCLI-D-14-00158.1.

Wang, C., S. Dong, A. T. Evan, G. R. Foltz, and S.-K. Lee, 2012: Multidecadal Covariability of North Atlantic Sea Surface Temperature, African Dust, Sahel Rainfall, and Atlantic Hurricanes. *J. Clim.*, **25**, 5404–5415, doi:10.1175/JCLI-D-11-00413.1.

Yuan, T., L. Oreopoulos, M. Zelinka, H. Yu, J. R. Norris, M. Chin, S. Platnick, and K. Meyer, 2016: Positive low cloud and dust feedbacks amplify tropical North Atlantic Multidecadal Oscillation: CLOUD AND DUST FEEDBACK AND AMO. *Geophys. Res. Lett.*, **43**, 1349–1356, doi:10.1002/2016GL067679.

663 Zhang, R., and T. L. Delworth, 2006: Impact of Atlantic multidecadal oscillations on India/Sahel
664 rainfall and Atlantic hurricanes. *Geophys. Res. Lett.*, **33**, doi:10.1029/2006GL026267.
665 http://doi.wiley.com/10.1029/2006GL026267 (Accessed September 21, 2016).

666 ——, R. Sutton, G. Danabasoglu, T. L. Delworth, W. M. Kim, J. Robson, and S. G. Yeager, 2016: Comment
667 on "The Atlantic Multidecadal Oscillation without a role for ocean circulation." *Science*, **352**,
668 1527–1527.

669 **Table 1 List of experiments**

Experiment Name	Model	Atmos. resolution	Ocean Type	Radiative Forcing	Extra NAO Forcing
1. CM2.1_Ctrl	CM2.1	~200 km	Dynamic	Constant 1860	None
2. CM2.1_Ctrl_NAO_50yr	CM2.1	~200 km	Dynamic	Constant 1860	50-year periodic
3. CM2.1_HIST	CM2.1	~200 km	Dynamic	Historical 1951-2014	None
4. CM2.1_HIST_NAO	CM2.1	~200 km	Dynamic	Historical 1951-2014	Observed 1951-2014
5. CM2.1_SLAB_Ctrl	CM2.1_SLAB	~200 km	50 m. Slab	Constant 1860	None
6. CM2.1_SLAB_HIST	CM2.1_SLAB	~200 km	50 m. Slab	Historical 1901-2014	None
7. CM2.1_SLAB_HIST_NAO	CM2.1_SLAB	~200 km	50 m. Slab	Historical 1901-2014	Observed 1901-2014
8. CM2.1_SLAB_Ctrl_NAO_50yr	CM2.1_SLAB	~200 km	50 m. Slab	Constant 1860	50-year periodic
9. FLOR_Ctrl	FLOR	~ 50 km	Dynamic	Constant 1860	None
10. FLOR_Ctrl_NAO_50yr	FLOR	~ 50 km	Dynamic	Constant 1860	50-year periodic
11. FLOR_HIST	FLOR	~50 km	Dynamic	Historical 1951-2014	None
12. FLOR_HIST_NAO	FLOR	~50 km	Dynamic	Historical 1951-2014	Observed 1951-2014
13. FLOR_SLAB_Ctrl	FLOR_SLAB	~50 km	50 m. Slab	Control 1990	None

670

671
672

673 **Figure Captions**
674
675 Figure 1 Zonal averages of the lagged correlations between annual mean SST and the NAO (for DJFM)
676 based on observations. Correlations were first computed at each grid point, and then zonally
677 averaged from 60^{o}W to 20^{o}W. Negative (positive) lags denote years prior to (after) a maximum in the
678 NAO. Lag zero indicates a correlation between the NAO (Dec, year 0 through Mar, year 1) with annual
679 mean SST (Jan, year 1 through Dec, year 1). (a) Correlations calculated using High Pass data (filtered
680 to retain time scales shorter than 10 years). (b) Correlations calculated using Low Pass data (filtered
681 to retain time scales longer than 10 years). For both (a) and (b) the stippling denotes points that do
682 not pass a statistical significance test (described in detail in the Appendix). The analyses shown here
683 were based on time series that were not detrended. Analyses using detrended time series produce
684 similar results, with somewhat larger correlations.
685
686 Figure 2 Figure 2 Maps of the correlation coefficient between observed annual mean SST at each grid
687 point and the NAO index. (a) Correlation coefficients between the DJFM NAO index and annual mean
688 SST in the immediately following year (Jan-Dec) using the High Pass filtered data. (b) Correlation
689 coefficients when annual mean SST lags the DJFM NAO index by 15 years using the Low Pass filtered
690 data. (c) Correlation coefficients between annual mean SST and the NAO using Low Frequency data
691 when the SST leads the NAO by 6 years. (d-h) Same as (c) for a lag of (0,6,12,18 and 24) years.
692 Correlations were computed without detrending (analyses using detrending produced similar results,
693 with somewhat larger correlations). Regions without stippling are significant at the 80% confidence
694 level using a two-sided Students-t test.
695

Figure 3 Zonal mean (60^0W-20^0W) of the correlation coefficient between simulated annual mean SST and the model's DJFM NAO index, calculated from various Control simulations. Data were time filtered prior to analysis. High Pass (HP) data retain only time scales shorter than 10 years, while Low Pass (LP) data contain only time scales longer than 10 years. Negative (positive) lags along the x-axis indicate years prior to (following) a maximum NAO value. A lag of zero year (dashed line) denotes a correlation coefficient calculated between the Dec-Mar NAO index and the mean SST for Jan-Dec, where the Jan-Mar period is the same for the NAO and SST. The stippling denotes points that do not pass a statistical significance test (described in detail in the Appendix).(a) HP output, CM2.1_SLAB. (b) LP output, CM2.1_SLAB. (c) HP output, FLOR_SLAB. (d) LP output, FLOR_SLAB. (e) HP output, CM2.1 (f) LP output, CM2.1, (g) HP output, FLOR, (h) LP output, FLOR.

Figure 4 Maps of the correlation coefficients between annual mean SST and the NAO index in various models. Each map is at a lag (in years) where the overall field of correlations is at a maximum. Positive lags indicate the NAO leading SST. LP (HP) indicates data have been filtered prior to the correlation analysis to retain time scales longer than (shorter than) 10 years.

Figure 5 (a) Normalized time series of the NAO (black) and associated heat flux time series (red) used as forcing in the idealized experiments. A positive (negative) phase of the NAO implies enhanced (reduced) ocean to atmosphere heat flux in the subpolar gyre. Negative values for heat flux indicate an enhanced ocean to atmosphere heat flux. (b) Zonal mean (60^oW-20^oW) of annual mean SST response (K) to NAO forcing in CM2.1_SLAB, calculated as SST in simulations with NAO forcing minus SST in simulations without NAO forcing. (c) Same as (b) for CM2.1. (d) Same as (b) for FLOR. (e) AMOC response to NAO forcing in CM2.1, calculated as the AMOC in simulations with NAO forcing

minus the AMOC in simulations without NAO forcing. Units are Sverdrups (1 Sv = $10^6 m^3 s^{-1}$) (f) Same as (e) but for FLOR model. (g) North Atlantic meridional ocean heat transport response (30°N) to NAO forcing in CM2.1 (black) and FLOR (red), calculated as the ocean heat transport in the simulations with the NAO forcing minus the ocean heat transport in the simulations without NAO forcing. An 11-year running mean was applied to results in (e)-(g).

Figure 6 Lead-lag correlations between the SST response and the imposed NAO forcing for the 50-year idealized NAO forcing experiments. The SST response was first calculated as the SST in the simulations with NAO forcing minus the SST in corresponding sections of the Control simulation. Linear correlations were computed at each grid point between the SST response and the imposed NAO forcing. The correlations were then zonally averaged over the domain 60°W-20°W. Regions with stippling do not pass a statistical significance test (using a resampling technique as described in the Appendix). (a) Results from CM2.1_SLAB_Ctrl_NAO_50yr. (b) Results from CM2.1_Ctrl_NAO_50yr . (c) Results from FLOR_Ctrl_NAO_50yr .

Figure 7 Lead-lag correlation analyses, similar to Figure 2f and 2h, using output from CMIP5 models (models were used that had Control simulations at least 300 years in length).

Figure 8 (a) Time series of observed NAO index (DJFM, station based index from https://climatedataguide.ucar.edu/climate-data/hurrell-north-atlantic-oscillation-nao-index-station-based). (b) Time series of anomalous flux forcing associated with imposed NAO anomalies. Time series shows annual mean flux anomalies averaged over 60°W-30°W, 50°N-60°N, after applying a seven–year running mean. (c) Observed annual mean SST anomalies averaged over 60°W-20°W,

742 30°N-65°N, after applying a 10-year low pass filer. Values plotted are anomalies with respect to time-
743 mean over 1951-1980. (d) Time series of annual mean SST response to NAO flux anomalies using
744 model CM2.1, calculated as SST in HIST_NAO minus SST in HIST. A 10-year low pass filtered was
745 applied to the output. (e) Similar to (d) using model FLOR. (f) Similar to (d) using model CM2.1_SLAB.
746
747 Figure 9 Annual mean SST differences, calculated as 1996-2005 time-mean (warm phase of AMO)
748 minus 1971-1985 time-mean (cold phase of AMO). Top panel: observations. Each of the bottom three
749 rows represent output from a model (FLOR, CM2.1, or CM2.1_SLAB). Each of the three columns
750 represents an experiment type. Left column: HIST. Middle column: HIST_NAO. Right column:
751 HIST_NAO minus HIST, thereby indicating the influence of the NAO. The left column should be
752 interpreted as the model-based estimate of the change in SST due to radiative forcing; the middle
753 column (except for observed panel at top) should be interpreted as the SST change induced by the
754 combined forcing of radiative changes and NAO changes. The right column should be interpreted as
755 the SST changes induced by NAO changes, calculated as the field in the middle column minus the field
756 in the left column.
757
758 Figure 10 Zonal mean (60^0W-20^0W) of the correlation coefficient between simulated annual mean
759 SST and the observed DJFM NAO index. The data were subject to a 10-year low pass filter prior to
760 analysis. (a) Results using ensemble of CM2.1_HIST_NAO simulations. (b) Results using ensemble of
761 CM2.1_HIST simulations. Stippled areas are not significant, using a similar technique as described in
762 the Appendix.
763
764

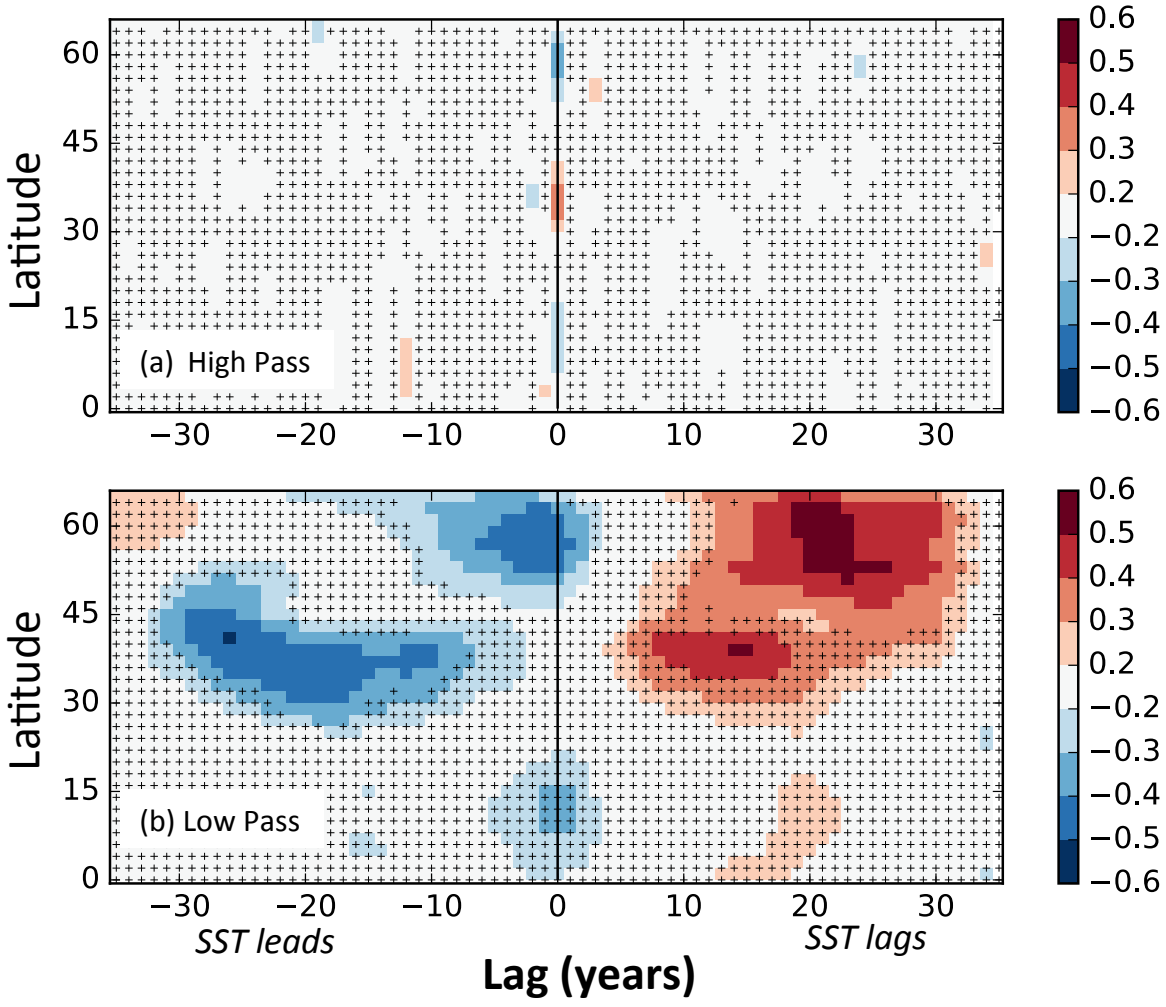

Figure 1 Zonal averages of the lagged correlations between annual mean SST and the NAO (for DJFM) based on observations. Correlations were first computed at each grid point, and then zonally averaged from 60°W to 20°W. Negative (positive) lags denote years prior to (after) a maximum in the NAO. Lag zero indicates a correlation between the NAO (Dec, year 0 through Mar, year 1) with annual mean SST (Jan, year 1 through Dec, year 1). (a) Correlations calculated using High Pass data (filtered to retain time scales shorter than 10 years). (b) Correlations calculated using Low Pass data (filtered to retain time scales longer than 10 years). For both (a) and (b) the stippling denotes points that do not pass a statistical significance test (described in detail in the Appendix). The analyses shown here were based on time series that were not detrended. Analyses using detrended time series produce similar results, with somewhat larger correlations.

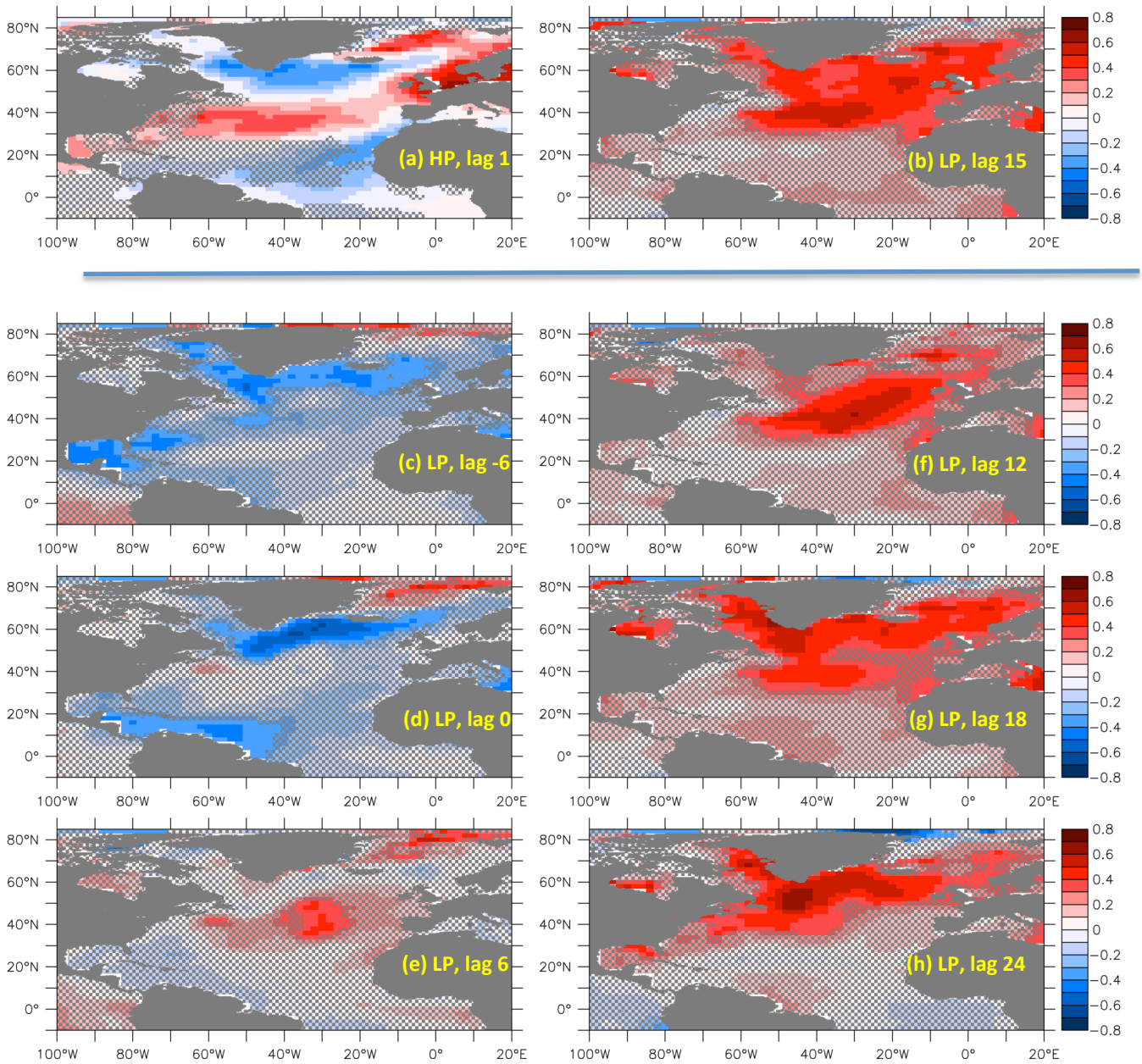

Figure 2 Maps of the correlation coefficient between observed annual mean SST at each grid point and the NAO index. (a) Correlation coefficients between the DJFM NAO index and annual mean SST in the immediately following year (Jan-Dec) using the High Pass filtered data. (b) Correlation coefficients when annual mean SST lags the DJFM NAO index by 15 years using the Low Pass filtered data. (c) Correlation coefficients between annual mean SST and the NAO using Low Frequency data when the SST leads the NAO by 6 years. (d-h) Same as (c) for a lag of (0,6,12,18 and 24) years. Correlations were computed without detrending (analyses using detrending produced similar results, with somewhat larger correlations). Regions without stippling are significant at the 80% confidence level using a two-sided Students-t test.

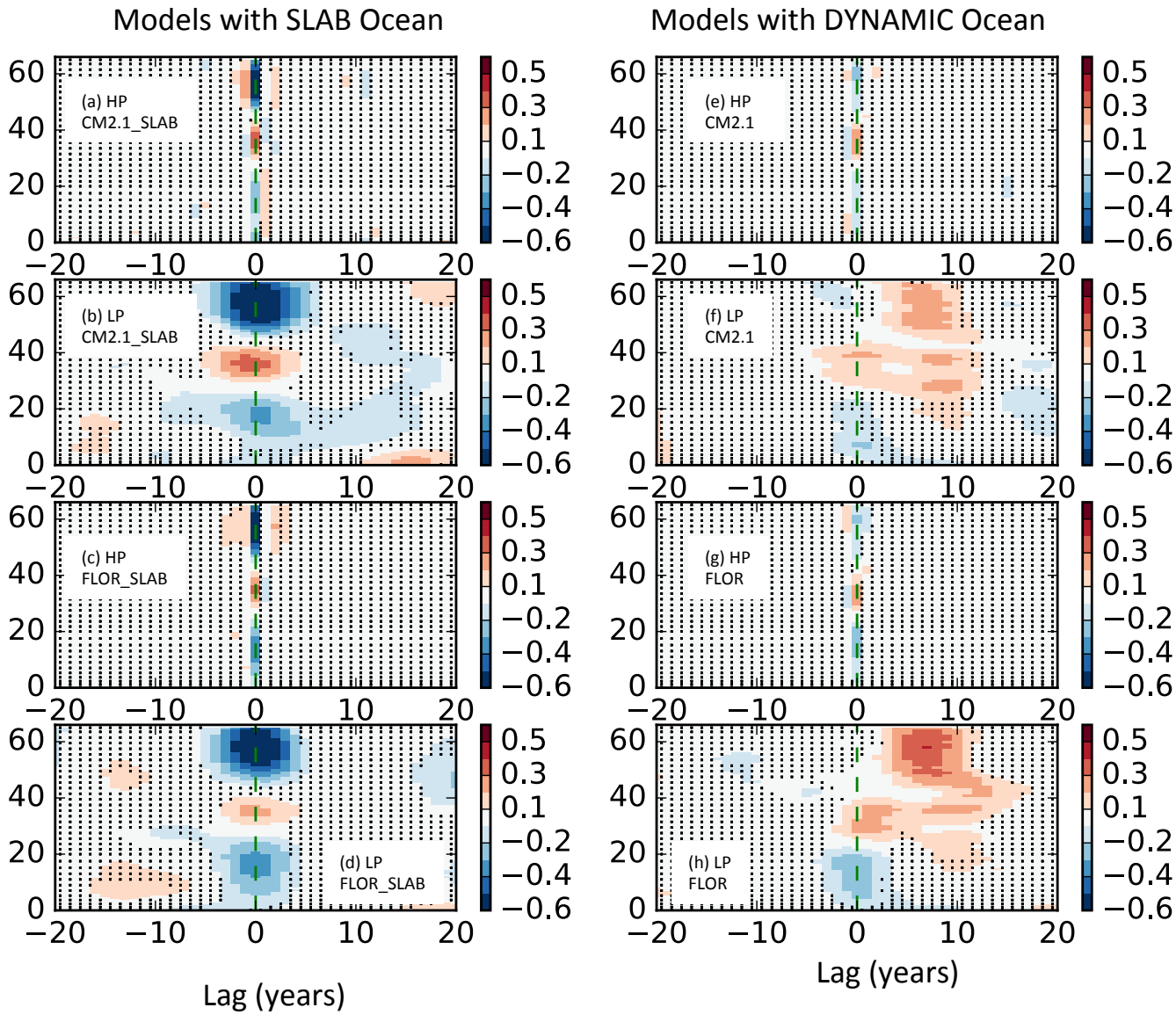

Figure 3 Zonal mean (60^{0}W-20^{0}W) of the correlation coefficient between simulated annual mean SST and the model's DJFM NAO index, calculated from various Control simulations. Data were time filtered prior to analysis. High Pass (HP) data retain only time scales shorter than 10 years, while Low Pass (LP) data contain only time scales longer than 10 years. Negative (positive) lags along the x-axis indicate years prior to (following) a maximum NAO value. A lag of zero year (dashed line) denotes a correlation coefficient calculated between the Dec-Mar NAO index and the mean SST for Jan-Dec, where the Jan-Mar period is the same for the NAO and SST. The stippling denotes points that do not pass a statistical significance test (described in detail in the Appendix).(a) HP output, CM2.1_SLAB. (b) LP output, CM2.1_SLAB. (c) HP output, FLOR_SLAB. (d) LP output, FLOR_SLAB. (e) HP output, CM2.1 (f) LP output, CM2.1, (g) HP output, FLOR, (h) LP output, FLOR.

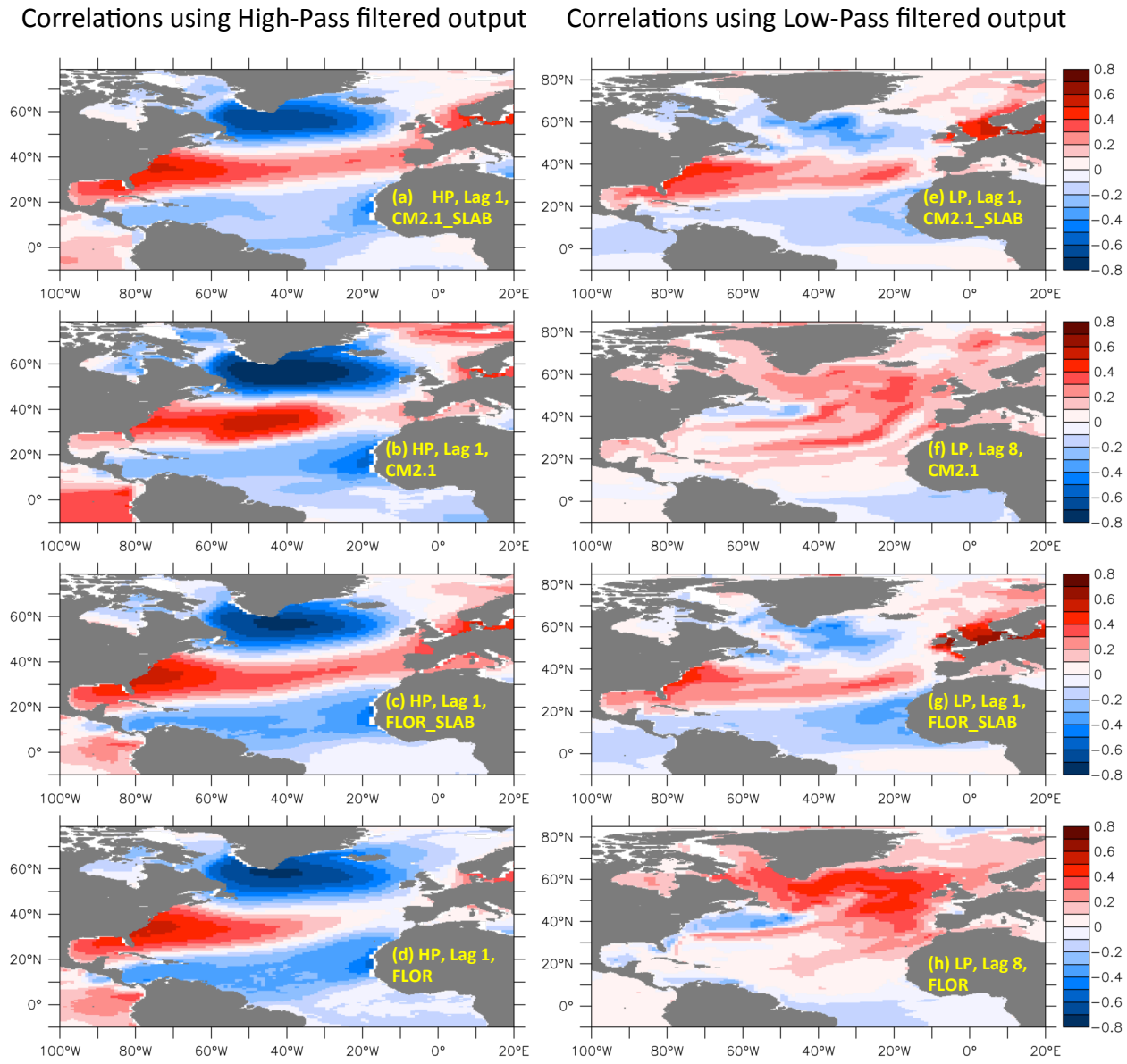

Figure 4 Maps of the correlation coefficients between annual mean SST and the NAO index in various models. Each map is at a lag (in years) where the overall field of correlations is at a maximum. Positive lags indicate the NAO leading SST. LP (HP) indicates data have been filtered prior to the correlation analysis to retain time scales longer than (shorter than) 10 years.

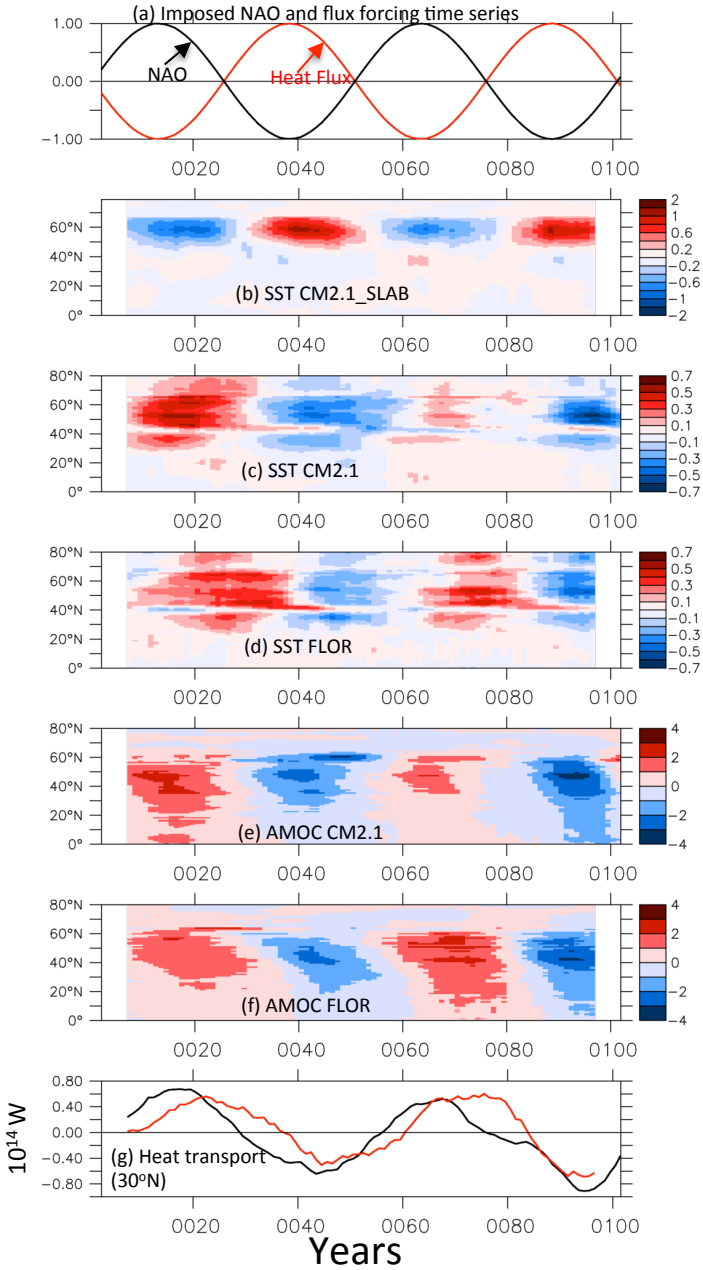

Figure 5 (a) Normalized time series of the NAO (black) and associated heat flux time series (red) used as forcing in the idealized experiments. A positive (negative) phase of the NAO implies enhanced (reduced) ocean to atmosphere heat flux in the subpolar gyre. Negative values for heat flux indicate an enhanced ocean to atmosphere heat flux. (b) Zonal mean (60°W-20°W) of annual mean SST response (K) to NAO forcing in CM2.1_SLAB, calculated as SST in simulations with NAO forcing minus SST in simulations without NAO forcing. (c) Same as (b) for CM2.1. (d) Same as (b) for FLOR. (e) AMOC response to NAO forcing in CM2.1, calculated as the AMOC in simulations with NAO forcing minus the AMOC in simulations without NAO forcing. Units are Sverdrups (1 Sv = $10^6 m^3 s^{-1}$) (f) Same as (e) but for FLOR model. (g) North Atlantic meridional ocean heat transport response (30°N) to NAO forcing in CM2.1 (black) and FLOR (red), calculated as the ocean heat transport in the simulations with the NAO forcing minus the ocean heat transport in the simulations without NAO forcing. An 11-year running mean was applied to results in (e)-(g).

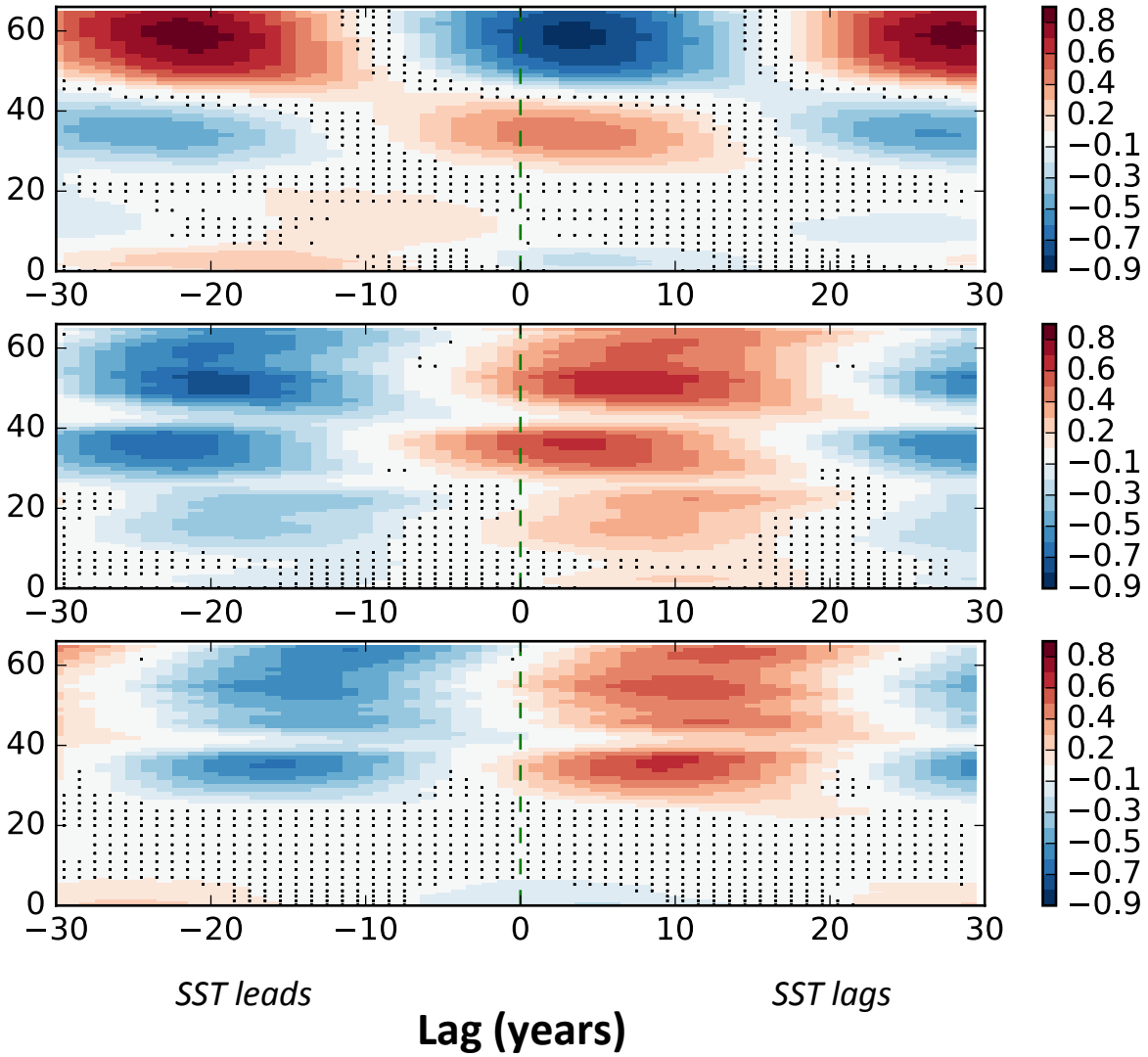

Figure 6 Lead-lag correlations between the SST response and the imposed NAO forcing for the 50-year idealized NAO forcing experiments. The SST response was first calculated as the SST in the simulations with NAO forcing minus the SST in corresponding sections of the Control simulation. Linear correlations were computed at each grid point between the SST response and the imposed NAO forcing. The correlations were then zonally averaged over the domain 60°W-20°W. Regions with stippling do not pass a statistical significance test (using a resampling technique as described in the Appendix). (a) Results from CM2.1_SLAB_Ctrl_NAO_50yr. (b) Results from CM2.1_Ctrl_NAO_50yr . (c) Results from FLOR_Ctrl_NAO_50yr .

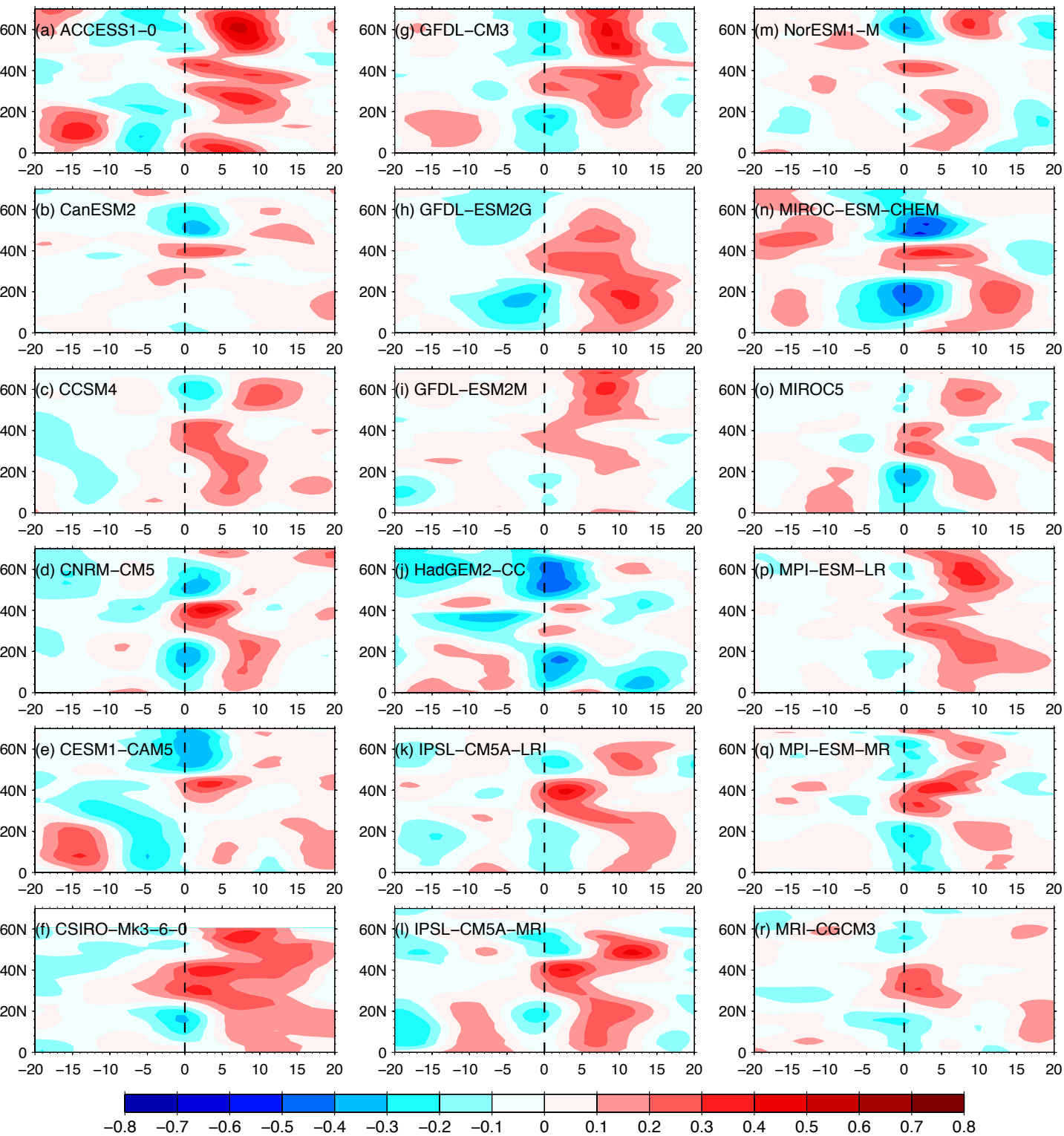

Figure 7 Lead-lag correlation analyses, similar to Figure 2f and 2h, using output from CMIP5 models (models were used that had Control simulations at least 300 years in length).

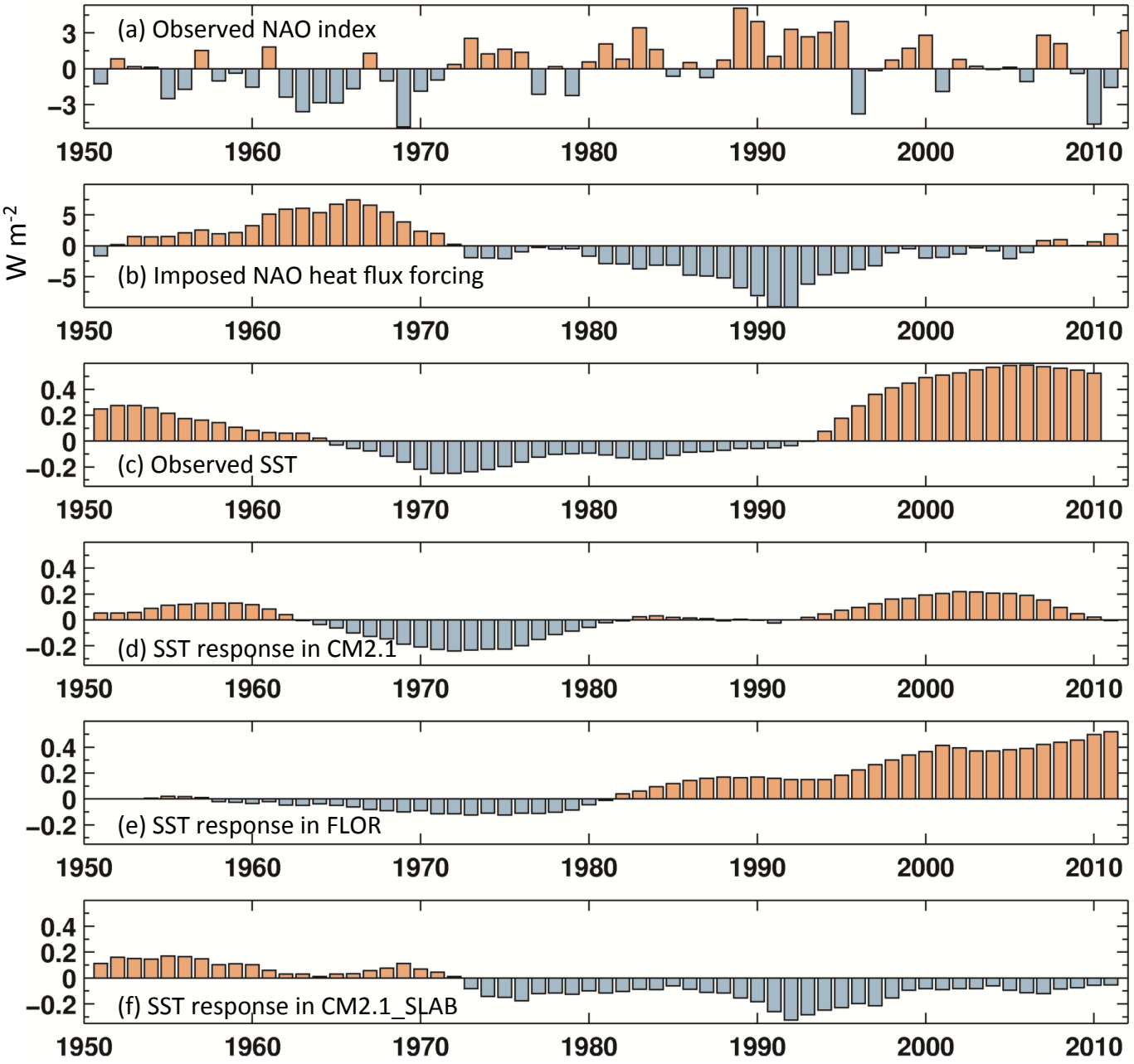

Figure 8 (a) Time series of observed NAO index (DJFM, station based index from https://climatedataguide.ucar.edu/climate-data/hurrell-north-atlantic-oscillation-nao-index-station-based). (b) Time series of anomalous flux forcing associated with imposed NAO anomalies. Time series shows annual mean flux anomalies averaged over 60°W-30°W, 50°N-60°N, after applying a seven–year running mean. (c) Observed annual mean SST anomalies averaged over 60°W-20°W, 30°N-65°N, after applying a 10-year low pass filer. Values plotted are anomalies with respect to time-mean over 1951-1980. (d) Time series of annual mean SST response to NAO flux anomalies using model CM2.1, calculated as SST in HIST_NAO minus SST in HIST. A 10-year low pass filtered was applied to the output. (e) Similar to (d) using model FLOR. (f) Similar to (d) using model CM2.1_SLAB.

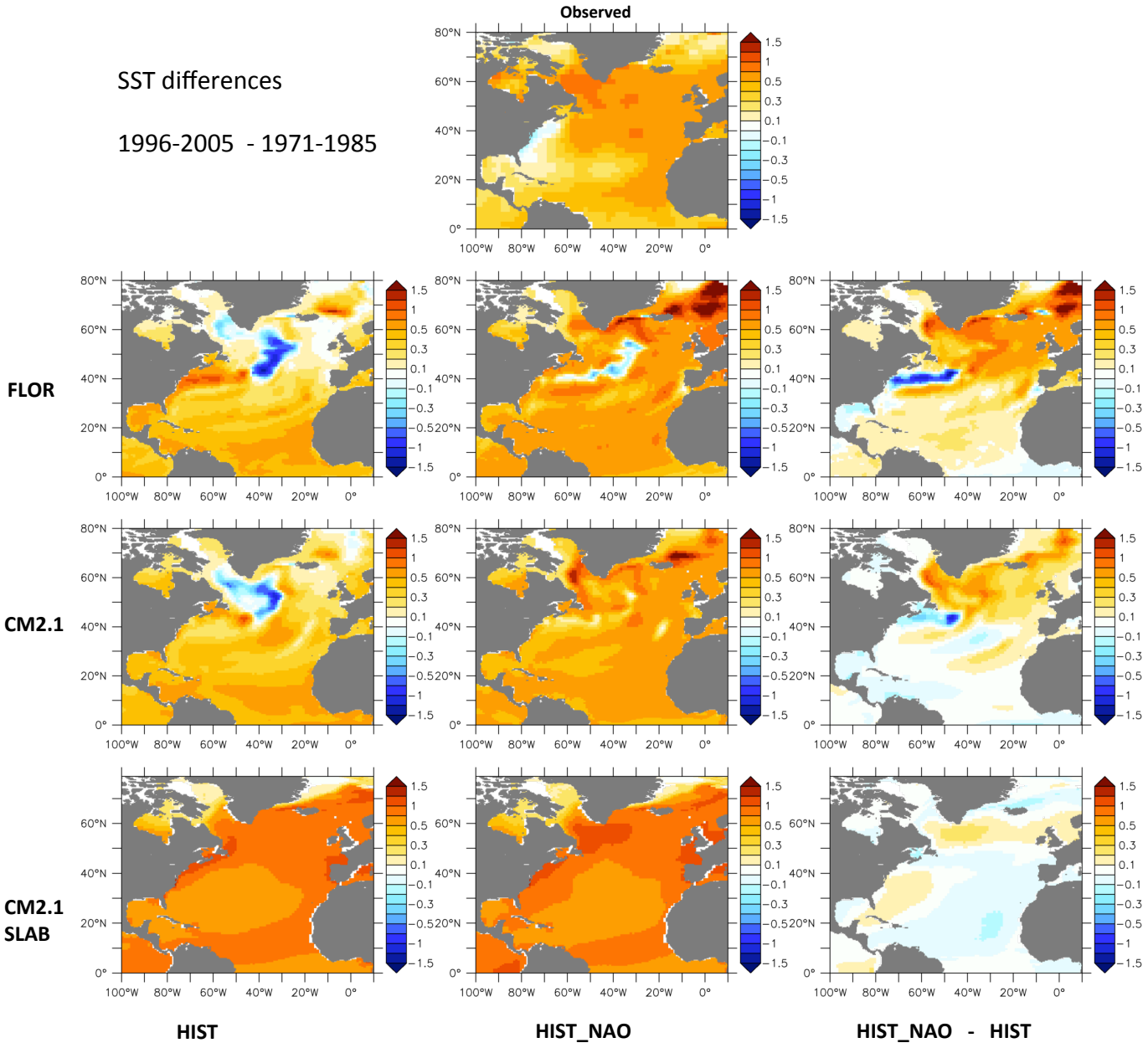

Figure 9 Annual mean SST differences, calculated as 1996-2005 time-mean (warm phase of AMO) minus 1971-1985 time-mean (cold phase of AMO). Top panel: observations. Each of the bottom three rows represent output from a model (FLOR, CM2.1, or CM2.1_SLAB). Each of the three columns represents an experiment type. Left column: HIST. Middle column: HIST_NAO. Right column: HIST_NAO minus HIST, thereby indicating the influence of the NAO. The left column should be interpreted as the model-based estimate of the change in SST due to radiative forcing; the middle column (except for observed panel at top) should be interpreted as the SST change induced by the combined forcing of radiative changes and NAO changes. The right column should be interpreted as the SST changes induced by NAO changes, calculated as the field in the middle column minus the field in the left column.

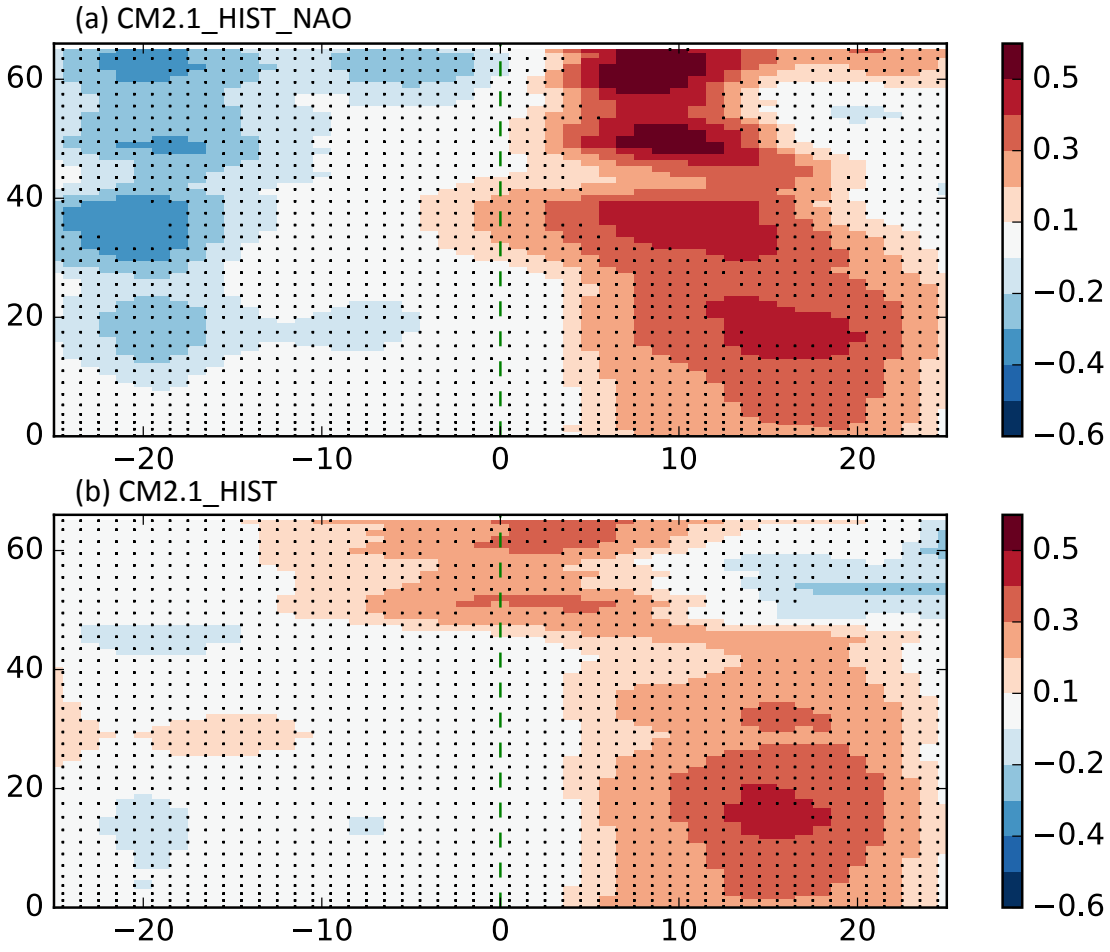

Figure 10 Zonal mean (60^0W-20^0W) of the correlation coefficient between simulated annual mean SST and the observed DJFM NAO index. The data were subject to a 10-year low pass filter prior to analysis. (a) Results using ensemble of CM2.1_HIST_NAO simulations. (b) Results using ensemble of CM2.1_HIST simulations. Stippled areas are not significant, using a similar technique as described in the Appendix.